Tuning the Photophysical Properties of Aza-BODIPYs in the Near-Infrared Region by Introducing Electron-Donating Thiophene Substituents

Thibaut Baron, Valentin Maffeis, Christophe Bucher, Boris Le Guennic, Akos Banyasz, Denis D Jacquemin, Gérard Berginc, Olivier Maury, Chantal Andraud

Chemistry–A European Journal
Research Article
doi.org/10.1002/chem.202301357
Chemistry Europe
European Chemical Societies Publishing
www.chemeurj.org

Tuning the Photophysical Properties of Aza-BODIPYs in the Near-Infrared Region by Introducing Electron-Donating Thiophene Substituents

Thibaut Baron,*[a] Valentin Maffeis,[a] Christophe Bucher,[a] Boris Le Guennic,[b] Akos Banyasz,[a] Denis Jacquemin,*[c, d] Gérard Berginc,[e] Olivier Maury,*[a] and Chantal Andraud[a]

Abstract: This study presents the synthesis, the spectroscopic and electrochemical properties of new bis- and tetra-substituted azaboron-dipyrromethene (aza-BODIPY) dyes substituted by different electron donating groups connected to the aza-BODIPY core through a thiophene unit. In line with theoretical calculations, experimental measurements point out the positive impact of the thiophene group that behave as a secondary donor group leading to an enhancement of the intramolecular charge transfer process in comparison to previously reported aza-BODIPY dyes. This heterocycle has also been found to tune the oxidative potential and to stabilize the electro-generated species.

Introduction

Selective near-infrared (NIR) absorbing dyes have received much attention due to their huge potential for a wide range of applications, spanning from materials to medical sciences, including bio- and photoacoustic imaging,[1,2] photodynamic therapy[3] and solar-to-electricity conversion with organic solar cells (OSCs)[4] or dye-sensitized solar cells (DSSCs).[5–8] A myriad of dye's families based on cyanines,[9] squaraines,[10] boron dipyrromethenes (BODIPYs),[11–14] pyrrolopyrroles, porphyrines, phtalocyanines[15] and rylenes[16] have already been developed for use in this spectral range.[17] During the past decade, our group focused on the design and synthesis of NIR dyes for multiphoton absorption based optical power limitation (OPL) in the short-wave infrared (SWIR) range and more precisely at the telecommunication wavelength (1550 nm).[17] In this context, reaching valuable nonlinear optical (NLO) properties requires to design specific molecular architectures, *i.e.*, dipolar or quadrupolar molecules containing electron-donating (EDG) and electron-withdrawing (EWG) groups linked through a π-conjugated system in order to promote effective photoinduced intramolecular charge transfer (ICT) processes.[18,19]

Meanwhile, Bouit *et al.* reported in 2009 the first study on the NLO and OPL behavior of the aza-BODIPY dye **Bdp1**^{b} (Figure 1).[20] Although these types of dyes have so far mostly been used as fluorescent probe for bioimaging or as active component for photodynamic therapy and for organic photovoltaics,[21] their robustness, their specific photophysical properties, *i.e.*, high extinction coefficient and fluorescence in the NIR region, and promising NLO in the SWIR, make them attractive candidates for OPL applications.[22] Furthermore, these dyes could be successfully incorporated in sol-gel materials leading to solid OPL devices.[23,24] The combination of optical characterizations and theoretical calculations has also revealed that the substitution of the central aza-BODIPY core, acting as a strong EWG, by one or several EDGs induces strong ICT transitions responsible for the enhanced spectroscopic and NLO properties. In this framework, the nature of the conjugated systems (phenylethynyl or fluorenylethynyl), as well as the positions of the donor units have been investigated, with substitution in 3,5 (bottom), 2,6 (lateral) and 1,7 (top) positions, as illustrated by dyes **Bdp1**^{b}, **Bdp1**^{t}, **Bdp1**^{l}, and **Bdp3**^{b} (see Figure 1).[22] The 3,5 functionalization (**Bdp1**^{b} and **Bdp3**^{b}) either with phenyl or extended fluorenyl-containing chromophore emerged as the most efficient strategy. Finally, we found that the double substitution (3,5 and 1,7) is actually the best strategy to improve simultaneously the two-photon absorption (2PA)

[a] *Dr. T. Baron, Dr. V. Maffeis, Dr. C. Bucher, Dr. A. Banyasz, Dr. O. Maury, Dr. C. Andraud*
Laboratoire de Chimie, UMR 5182
ENS Lyon, CNRS, Université Lyon 1
46 Allée d'Italie, 69364 Lyon (France)
E-mail: thibaut.baron@ens-lyon.fr
olivier.maury@ens-lyon.fr
[b] *Dr. B. Le Guennic*
Univ Rennes, CNRS
ISCR (Institut des Sciences Chimiques de Rennes)
UMR 6226, 35000 Rennes (France)
[c] *Prof. D. Jacquemin*
Nantes Université, CNRS, CEISAM, UMR-6230
44000, Nantes (France)
E-mail: Denis.Jacquemin@univ-nantes.fr
[d] *Prof. D. Jacquemin*
Institut Universitaire de France (IUF)
75005, Paris (France)
[e] *Dr. G. Berginc*
Thales LAS France
2 Avenue Gay Lussac, 78990 Élancourt (France)

Supporting information for this article is available on the WWW under https://doi.org/10.1002/chem.202301357

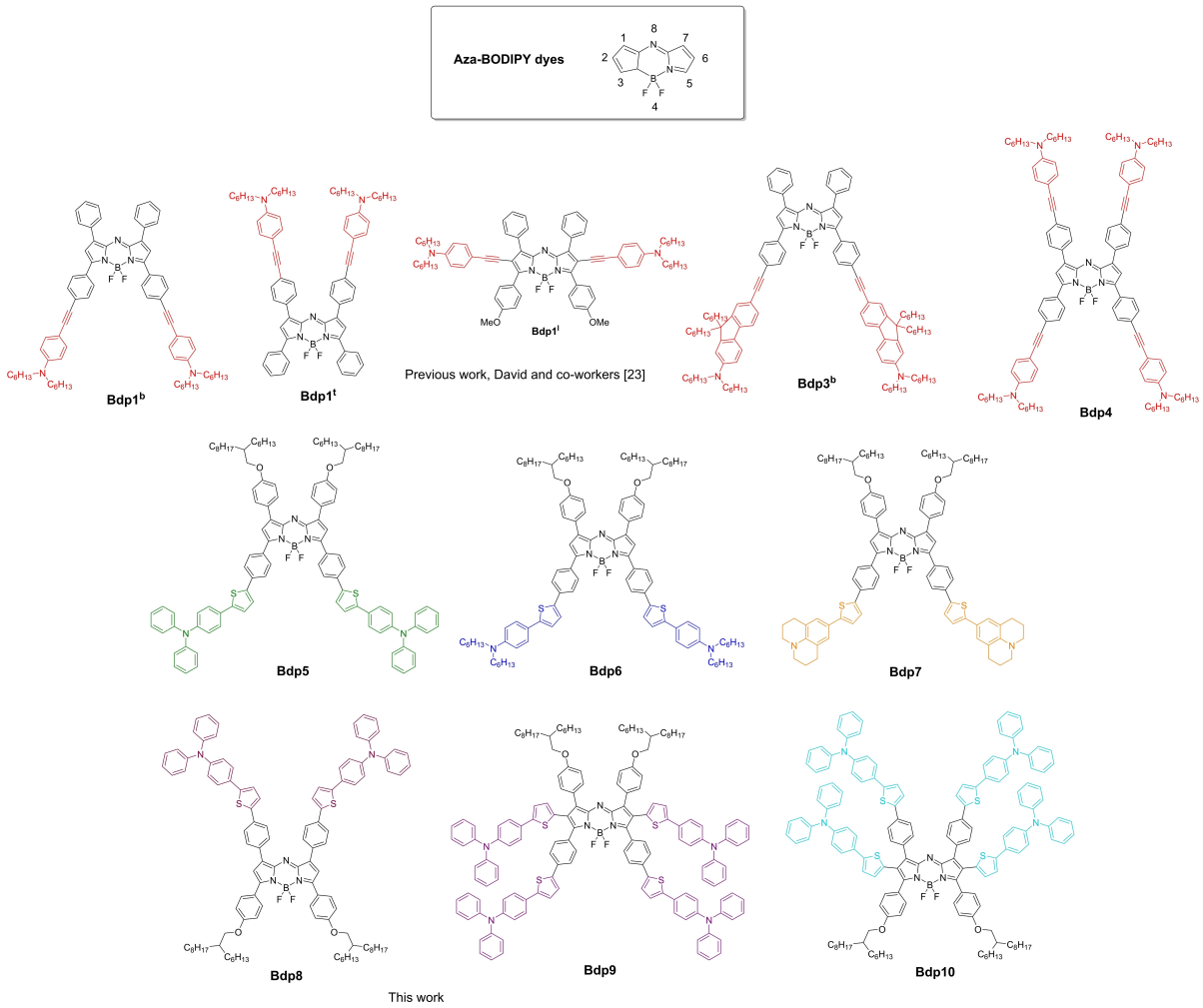

Figure 1. Structures of previously published aza-BODIPY dyes **Bdp1^{b}**, **Bdp1^{t}**, **Bdp1^{l}**, **Bdp3^{b}**, and **Bdp4** designed for OPL at telecommunication wavelength and the new **Bdp5-10** dyes investigated herein.

and excited state absorption properties leading to the best OPL behavior (**Bpd4** in Figure 1) of this series.[22] However, the overall synthetic yield of these doubly-substituted dyes is generally very low which limits their practical use as concentrated active dyes in bulk sol-gel devices.

More recently, it has been proposed to replace the phenyl substituents at positions 1,7 with benzothiazoles (BTDs) in order to maximize the ICT. Those BTD-substituted aza-BODIPYs are among the most red-shifted fluorescent dyes reported to date.[25,26] However, in spite of remarkable OPL efficiency in solution in the SWIR,[26] these molecules could not be used as solid optical limiters, due to their impossible incorporation into sol-gel matrices. Another strategy consists in tuning the spectroscopic properties of aza-BODIPY dyes by replacing the phenyl moieties with thiophene, which was found to result in a bathochromic shift of the absorbance and an increase of the molar extinction coefficient.[27,28] It is also well-known that using thiophene as π-bridges increases the biphotonic absorption properties thanks to its lower aromaticity and stronger donating effect than phenyl.[29]

Herein, we describe the straightforward syntheses of six new aza-BODIPY derivatives, including the bis-substituted dyes **Bdp5-8** and the tetra-substituted dyes **Bdp9-10** (Figure 1), bearing different EDGs connected to the aza core through a thiophene linker. In the targeted compounds, the thiophene unit is directly introduced at the 3,5 and 2,6 positions of the aza-core to ensure good electronic communication between the EDGs and EWGs. The impact of thiophene can also be directly compared to the previously reported reference compound **Bdp1^{b}** incorporating an ethynyl bridge. In addition, we studied the impact of the position (3,5 versus 2,7) and the nature of the donors (triarylamine, dialkylaniline, and julolidine) on the properties. All dyes were thoroughly characterized by absorption and fluorescence spectroscopy, electrochemistry (EC) and spectro-electrochemistry (SEC) measurements supported by theoretical calculations to analyze the interplay between structural modifications and ICT, π-electronic conjugation, and stability of the redox species.

Synthesis

In order to prepare the targeted aza-BODIPY derivatives (**Bdp5-10**, Figure 1) bearing EDGs connected to thiophene units, we firstly synthesized the aza-dipyrromethene **1** and **2** substituted with bromine at the low and top positions of the BODIPY skeleton, respectively (Scheme 1). Their syntheses were carried out following the procedure described by O'Shea et al. involving a chalcone intermediate (Scheme S1).[30] Both intermediates are also substituted by hexadecyloxy side chain to ensure optimal solubility.[31] In contrast to previous reports where the EDGs were introduced via Sonogashira cross-coupling,[20,22] we performed Stille cross-coupling to functionalize the aza-dipyrromethenes **1** and **2**. This approach is quite original, as evidenced by the limited number of BODIPYs obtained using this method.[32] For this reason, we have first prepared the stannic donors $\mathbf{D_1}$, $\mathbf{D_2}$, and $\mathbf{D_3}$, (Scheme S2–4) which differ by the nature of the peripheral amine moieties only, for example, triarylamine, dialkylaniline, and julolidine. The synthesis of $\mathbf{D_1}$ starts from the commercially available 4-bromotriphenylamine which, after substitution of the bromine by a boron pinacol ester, was further engaged in a Suzuki cross-coupling reaction with the 2-bromothiophene to yield $\mathbf{D_1}'$ with a 68% yield (Scheme S2). Both $\mathbf{D_2}'$ and $\mathbf{D_3}'$ donors were prepared using Stille couplings (Schemes S3 and S4). Finally, the insertion of -$SnBu_3$ affording donors $\mathbf{D_1}$, $\mathbf{D_2}$, and $\mathbf{D_3}$ was achieved by metal-exchange reactions using *n*-BuLi and Bu_3SnCl at low temperature.[33]

The aza-dipyrromethenes **1** and **2** were further engaged in palladium-catalyzed Stille cross-coupling reactions with an excess of donors to obtain the targeted di-substituted dipyrromethene **3**, **4**, **5**, and **6** (Scheme 1). We can notice that the reactivity is different depending on the bromine position: the yields are relatively good (higher than 65%) when the coupling is performed at the 3,5-positions while it is low when substitution occurs at the 1,7-positions of the aza core. More importantly, all compounds (from **3** to **6**) showed a good solubility, allowing easy purifications by flash chromatography. Final complexation was achieved using $BF_3.Et_2O$ and Hünig's base to afford the desired di-substituted aza-BODIPYs **Bdp5-8** with high yields (68 to 99%).

We then extended this approach to the tetra-brominated reagents **7** and **8**, prepared via an additional bromination of intermediates **1** and **2** using $TBABr_3$ (Scheme 2).[26,34] Following the above-described procedure, **7** and **8** were engaged in tetra-Stille coupling reactions using donor $\mathbf{D_1}$ and tetrakis (triphenylphosphine) palladium to afford the targeted dipyrromethene **9** and **10**. Intermediate **9** was obtained with a high yield (80%) indicating that the additional substitution on the side positions does not alter the reactivity. On the other hand, as previously observed for **6**, the yield was found to be lower when substitution occurs at the low positions of the aza-BODIPY core, as demonstrated by obtaining intermediate **10** in only 34% yield. Those two aza-dipyrromethenes were ultimately complexed with $BF_3.Et_2O$ to afford the desired products **Bdp9** and **Bdp10** in quantitative yields. It should be mentioned that these two compounds are the first examples of tetra-functionalization (top/bottom and lateral positions) of an aza-BODIPY core by strong EDGs and pave the way for many future possibilities of functionalization. In addition, these reactions were generally achieved without particular difficulties on over 100 mg scales leading to highly soluble derivatives, easy to purified by column chromatography.

Spectroscopic properties

The electronic absorption and emission spectra of **Bdp5-10**, measured in cyclohexane are presented in Figure 2. Furthermore, their photophysical properties, *i.e.*, wavelengths of maximum absorbance (λ_{abs}), emission wavelengths (λ_{em}), molar extinction coefficients (ε), fluorescence lifetimes (τ_{em}) and emission quantum yields (Φ) are collected in Table 1 but more

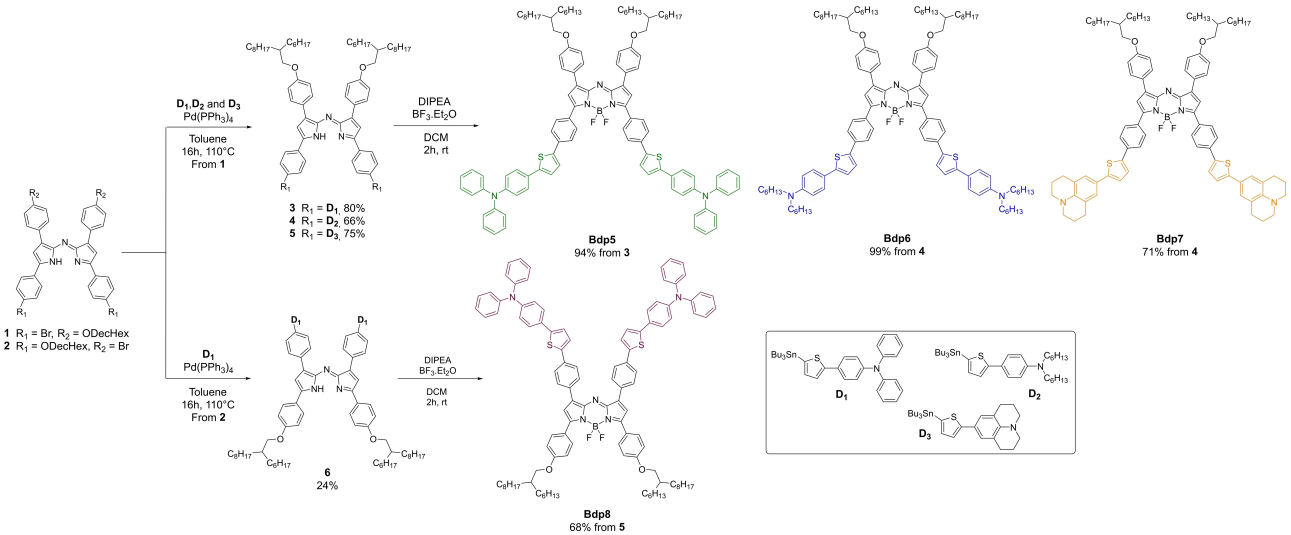

Scheme 1. Synthesis of aza-BODIPYs **Bdp5-8** via Stille cross-coupling reaction.

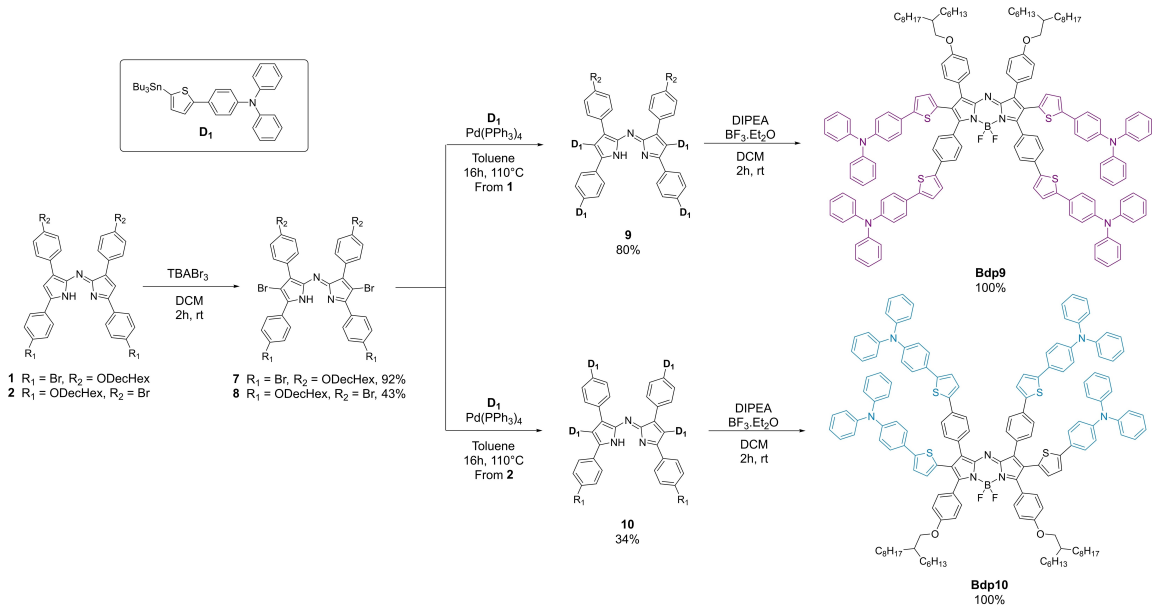

Scheme 2. Synthesis of the tetra-substituted aza-BODIPYs **Bdp9** and **Bdp10**.

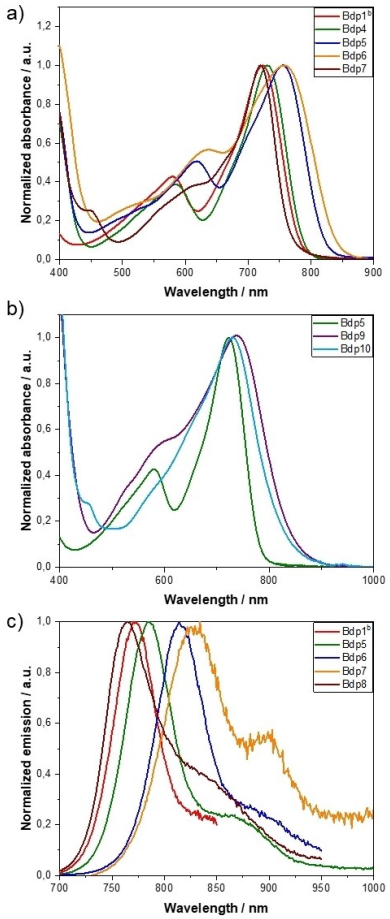

Figure 2. Normalized a) absorption and c) emission spectra of **Bdp1**^{b} (red), **Bdp5** (green), **Bdp6** (blue), **Bdp7** (orange) and **Bdp8** (wine), b) absorption of **Bdp5** (green), **Bdp9** (violet) and **Bdp10** (cyan) recorded in cyclohexane solution at room temperature.

data can be found in the Supporting Information (Figures S1–7, Tables S1–3).

All the di-substituted derivatives **Bdp5**, **Bdp6**, **Bdp7**, and **Bdp8** feature the classical spectroscopic signature of aza-BODIPYs dyes including an intense absorption band in the NIR region resulting in strong blue-green colorations (Figure 2).[22] This lower energy band is rather broad and is accompanied by a shoulder at higher energy. The additional intense transition observed at about 400 nm has been attributed to a localized π-π* electronic transition centered on the aniline fragment.[22] Interestingly, we found that the two lower energy transitions are sensitive to the solvent polarity, as revealed by the bathochromic and hyperchromic shifts observed when the polarity of the solvent increases, suggesting a partial ICT character of the transition (Figure S1 and Table S1). All compounds are emissive in cyclohexane and **Bdp5** also exhibits fluorescence in toluene (Figure S2). When increasing the solvent polarity from cyclohexane to toluene the quantum yield decreases, and emission even vanishes in dichloromethane, chloroform, and THF (Figures S3–4). More precise assignment of all transitions has been achieved with the help of theoretical calculations (see bellow). As already observed,[22] the role of the substitution position is significant with a blueshift of **Bdp8** substituted with donor **D**$_1$ in top position compared to **Bdp5** (Figure 2a). The lifetime and the quantum yield are also lower and these effects can be explained by the absence of fluorine-hydrogen interaction that rigidifies the structure and increases the conjugation when the donor is located in 3,5 positions.[35]

Comparison between **Bdp6** and the benchmark **Bdp1**^{b}, featuring two dialkylaniline EDGs, allowed us to evaluate the impact of the new conjugated bridge. We found that replacing the triple bond by a thiophene moiety results in a significant bathochromic shift of the lower energy transition ($\Delta\lambda_{abs}$ = 34 nm–620 cm^{-1}), consistent with the extension of conjugation

Table 1. Wavelength of maximal absorption (λ_{abs}) with extinction coefficient (ε), full-width at half-maximum ($\omega_{1/2}$), wavelength of maximal emission (λ_{em}), zero-zero energy level of the lowest excited state (E_{00}), electron lifetime (τ) and quantum yield of fluorescence (Φ) in cyclohexane for **Bdp1**[b] and **Bdp5-10**.

Dye	λ_{abs} [nm][a] (ε [$M^{-1}cm^{-1}$])	$\Delta\lambda_{abs}$ [nm][b] ([cm^{-1}])	$\omega_{1/2}$ [cm^{-1}]	λ_{em} [nm]	$\Delta\lambda_{em}$ [nm][c] ([cm^{-1}])	E_{00} [eV]	τ_{em} [ns]	Φ [%]
Bdp1[b]	722 (65000)	–	1700	773	–	1.66	–	18
Bdp5	730 (87500)	8 (150)	1600	786	9 (210)	1,63	2.58	24
Bdp6	756 (78400)	34 (620)	2100	814	41 (650)	1.57	1.98	13
Bdp7	758 (61100)	36 (660)	4100	829	56 (870)	1.55	1.38	2
Bdp8	720 (75800)	−2 (−40)	1700	764	−9 (−150)	1.67	2.01	18
Bdp9	735 (55500)	13 (240)	5400	–	–	–	–	-
Bdp10	730 (54200)	8 (150)	3200	–	–	–	–	-

[a] Determined in toluene. [b] Calculated according to the equation: λ_{abs} (**Bdpn**)-λ_{abs} (**Bdp1**[b]), n = 5, 6, 7 and 8. [c] Calculated according to the equation: λ_{em} (**Bdpn**)-λ_{em} (**Bdp1**[b]), n = 5, 6, 7 and 8.

and with the auxiliary electron donor character of this heterocycle. The same is found for the emission spectra with a rather large redshift ($\Delta\lambda_{em}$ = 41 nm–650 cm^{-1}) and small decrease of the quantum yield from 18 to 13%. We have also analyzed the influence of the nature of the EDGs by comparing **Bdp5**, **Bdp6**, and **Bdp7** featuring triarylamine, dialkylaniline, and julolidine moieties, respectively. Due to the increase of the electron donating character (triarylamine < dialkylaniline < julolidine), the diphenylamine-substituted dye **Bdp5** was found to exhibit the most blue-shifted emission signals (by about 27 nm from that recorded with **Bdp6** and **Bdp7**). This effect is even more pronounced in the case of the second transition assigned to an ICT band. The emission spectra recorded in cyclohexane follow the same trends as above (Figure 2c) with maximum fluorescence wavelengths shifted in the NIR at 786, 814 and 829 nm for **Bdp5**, **Bdp 6**, and **Bdp7**, respectively. This shift is accompanied by a decrease of the fluorescence quantum yield from 18 to 2% in cyclohexane.

Finally, the tetra-substituted aza-BODIPYs **Bdp9** and **Bdp10** exhibit much broader absorption bands, $w_{1/2}$ = 5400 and 3200 cm^{-1} respectively, with maxima located at 735 and 730 nm compared to the di-substituted analogues **Bdp5** (730 nm, 1600 cm^{-1}) and **Bdp8** (720 nm, 1700 cm^{-1}). In contrast, the emission of **Bdp9** and **Bdp10** is completely quenched even in cyclohexane.

In an attempt to capture the process behind the solvatochromic fluorescence quenching and hypochromic shift, we performed two-photon excited fluorescence (TPEF) measurements using different solvent mixtures of increasing polarity (see Figures 2 and S8–9). We state that the choice of laser TPEF was practically motivated to combine the efficiency of 2PA and higher sensitivity of our TPEF setup compared to classical fluorimeter (see Supporting Information for more details). Adding dichloromethane to a solution of **Bdp5** in toluene resulted in a large and continuous bathochromic shift (550 cm^{-1} (40 nm) at 100:50 v/v) and broadening of the fluorescence band (Figure 2a) associated with a moderate fluorescence quenching (98% at 100/50 v/v). Once again, the signature of **Bdp5** was found to be less solvent dependent than the other dyes of the series, in part due to the presence of weaker EDGs which results in a mild ICT. At high dichloromethane ratio, the typical cyanine emission observed in cyclohexane and toluene becomes a large highly symmetric band retaining a few percent of the fluorescence intensity (Figure 3c). Our hypothesis is that the ICT character of the stabilized excited state of **Bdp5** slightly increases with the increasing polarity of the solvent resulting in a typically broader and less intense emission.

Both **Bdp6** and **Bdp7** show a large dependence to the solvent polarity: adding dichloromethane to cyclohexane solutions results in huge bathochromic shifts (around 950 cm^{-1} (80 nm) for 100/50 v/v, see Figure 3b and S8a) and large band

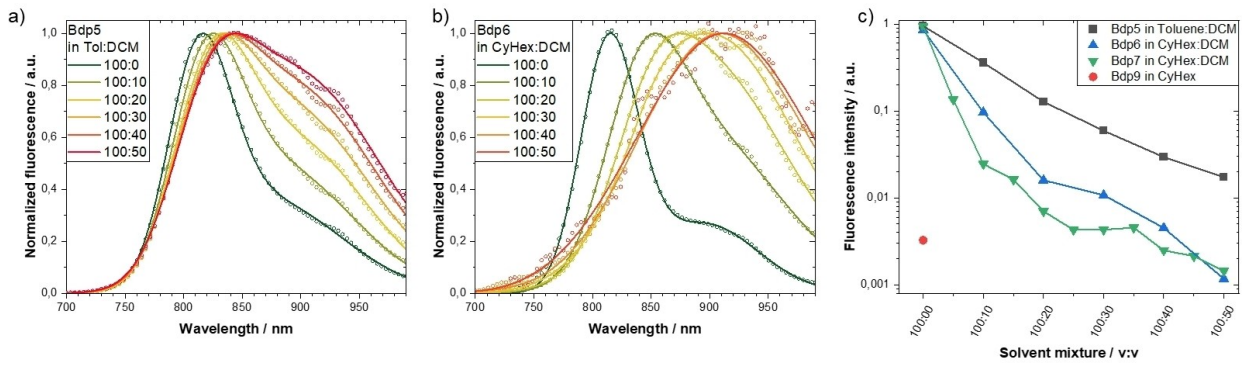

Figure 3. Two-photon excited fluorescence, excitation at 1100 nm, 100 mW for different solvent ratio for a) **Bdp5** in a mixture of toluene and dichloromethane and b) **Bdp6** in a mixture of cyclohexane and dichloromethane and c) evolution of the relative fluorescence intensity for **Bdp5** (black, square), **Bdp6** (blue, upward triangle), **Bdp7** (green, downward triangle) and **Bdp9** (red, circle) for different solvent mixture. The reader is advised of the logarithm scale.

broadenings. The quenching of the fluorescence is stronger than for **Bdp5** (Figure 3c) and larger for **Bdp7** than for **Bdp6** coincidently to the increasing strength of their EDG. This ordering corresponds to the computed ICT strengths for these three compounds (see below). We hypothesize that the Franck-Condon state of these molecules possess a dominant cyanine character with a small ICT ability but that its conversion towards another relaxed excited state with a ICT character is permitted when the latter is energetically stabilized in highly polar environment resulting in redshifted (stabilized), broad and less intense (ICT character) fluorescence band. Such behavior has been largely reported for push-pull dyes.[36–39] This aspect was also explored with theory (see below).

At the limit of our sensitivity, we could observe the fluorescence of **Bdp9** in pure cyclohexane (see Figure S8b). Interestingly, the shape of the band is that of a typical cyanine emission with a mean band position at 850 nm. Therefore, we attribute this signal to the few photons emitted from the directly excited Franck-Condon state. This excited state is certainly bright, but steadily quenched. By analogy with **Bdp5**, **Bdp6**, and **Bdp7**, we favor the hypothesis of a low-energy dark state with an ICT nature. Femtosecond absorption spectroscopy would be needed to shed light to the exact excited state relaxation mechanism.

Electrochemical measurements

The electrochemical properties of the **Bdp** dyes were investigated by cyclic voltammetry measurements using a carbon disk working electrode and an Ag^+/Ag ($AgNO_3$ 10^{-2} M in acetonitrile) reference electrode (Figure 4 and S10). All measurements were carried out under N_2 in 1,2-dichloroethane containing 0.1 M tetra-*n*-butylammonium perchlorate (TBAP) used as supporting electrolyte. Selected potential values collected with these compounds are listed in Table 2. Those studies revealed that **Bdp1[b]-10** exhibit similar signatures in the cathodic domain, with two successive one-electron reduction waves observed between −0.70 and −1.45 V attributed to the successive formation of **Bdp$^{-\bullet}$** and **Bdp^{2-}**. The poor stability of **Bdp^{2-}** compared to **Bdp$^{-\bullet}$** was first revealed by the irreversibility of the second reduction wave at all investigated scan rates. Only the first reduction wave was found to exhibit reversible features at 100 mV.s^{-1}. The half-wave and peak potential values ($E_{1/2}$ [**Bdp/Bdp$^{-\bullet}$**] and E_p [**Bdp$^{-\bullet}$/Bdp^{2-}**]) collected for all compounds in the series fall within the same range as those previously reported for parent phenyl- and OMe-substituted aza-BODIPYs, which confirms that the reduction processes are centered on the aza-BODIPY core and that the bis or tetra-substitution with EDGs has a limited effect on the potential values.[40,41]

Greater differences were observed in the series on the anodic side. As can be seen in Figure 3, the CV curves recorded at 100 mV.s^{-1} for **Bdp**n (n = 5, 6, 8, 9, 10) feature two successive reversible oxidation waves with very different intensities. The number of electrons exchanged in each process was assessed

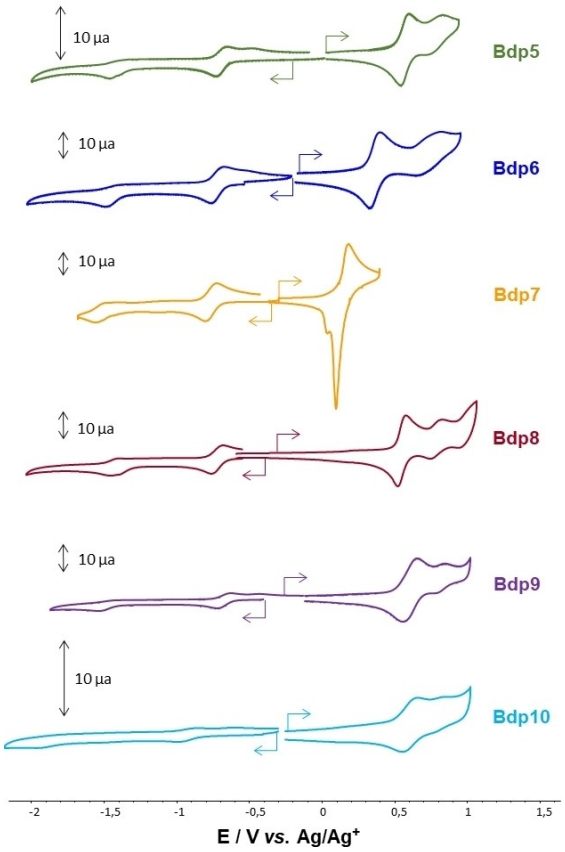

Figure 4. Voltammetric curves of dichloroethane solutions of **Bdp5** (green), **Bdp6** (blue), **Bdp7** (orange), **Bdp8** (wine), **Bdp9** (purple) and **Bdp10** (cyan) (5×10^{-4} M + 0.1 M) recorded at a vitreous carbon working electrode (Ø = 3 mm, *E* (V) vs $AgNO_3$/Ag (10^{-2} M), v = 0.1 V.s^{-1}).

Table 2. Anodic and cathodic peak potentials (E_{pa}, E_{pc}) and half-wave potentials ($E_{1/2}$) values (V) measured by CV for **Bdp1[b]**, **Bdp5**, **Bdp6**, **Bdp7**, **Bdp8**, **Bdp9** and **Bdp10** in dichloroethane containing 0.1 m TBAP at a vitreous carbon electrode (Ø = 3 mm, v = 0.1 V.s^{-1}), *E* vs $AgNO_3$/Ag (10^{-2} in ACN). Red_n and Ox_n represent the nth successive reduction and oxidation processes, respectively.

Dye	Red_2 E_{pc} [V]	Red_1 E_{pa} [V]	E_{pa} [V]	$E_{1/2}$ [V]	Ox_1 E_{pa} [V]	E_{pc} [V]	$E_{1/2}$ [V]	Ox_2 E_{pa} [V]
Bdp1[b]	−1.43	−0.63	−0.71	−0.67	0.54	–	–	–
Bdp5	−1.45	−0.66	−0.73	−0.70	0.63	0.54	0.58	0.83
Bdp6	−1.46	−0.67	−0.75	−0.71	0.40	0.34	0.37	0.81
Bdp7	−1.53	−0.70	−0.77	−0.74	0.17	–	–	–
Bdp8	−1.42	−0.66	−0.74	−0.70	0.57	0.52	0.54	0.82
Bdp9	−1.51	−0.62	−0.70	−0.66	0.66	0.55	0.60	0.84
Bdp10	−1.40	−0.62	−0.70	−0.66	0.64	0.56	0.60	0.82

from the relative intensity of the corresponding diffusion limited current measured in stationary regime using a rotating disk electrode (red curve in Figure S10). These differences led us to assign the second wave to the one electron oxidation of the aza-BODIPY skeleton and the first one to a two-electron oxidation of the arylamine substituents (one electron per arylamine). The standard shape of the first oxidation wave is moreover consistent with the conclusion that there is no communication between the two amine substituents neither through space nor through bonds. We also found that the half wave potential calculated for the first oxidation wave ($E_{1/2}$ in Table 2) is strongly influenced by the nature of the amine group introduced on the aza-BODIPY core. The values collected in Table 2 bring to light that the oxidation of the julolidine (**Bdp7**), dialkylaniline (**Bdp**n with n = 1, 4, 6) and triarylamine (**Bdp**n with n = 5, 9, 10) moieties are observed at 0.17, 0.40, and 0.58 V respectively, which is in agreement with the relative basicity of those amines.[21,42]

Comparing the electrochemical signatures of **Bdp1**[b] and **Bdp6** (Figure S10) then showed that the thiophene units make the dyes easier to oxidize and stabilize the oxidized forms, as proved by the reversible character of the waves recorded at 100 mV.s^{-1} for all the thiophene-containing dyes. The stabilization of the cation radicals is thus most likely due to a modification of the charge distribution and spin density through a combination of conjugative and inductive effects resulting from the presence of thiophene EDGs.[43] The shift of the first reduction wave was also used as a probe allowing to compare the electronic effects of the julolidine, triarylamine and dialkylaniline substituents introduced at the 3,5 or 2,6-positions of the aza-BODIPY core. We found that the reduction potential associated to the first reversible wave undergoes a progressive cathodic shift in the following order $E_{1/2}$(**Bdp9**) ~ $E_{1/2}$(**Bdp10**) > $E_{1/2}$(**Bdp1**) > $E_{1/2}$(**Bdp8**) ~ $E_{1/2}$(**Bdp5**) > $E_{1/2}$(**Bdp6**) > $E_{1/2}$(**Bdp7**). Restricting this comparison to dyes incorporating two EDGs, namely **Bdp5-8**, allowed us to confirm that the julolidine substituent is a much stronger donor than dialkylaniline and triarylamine. The 10 mV difference observed between $E_{1/2}$(**Bdp5**) and $E_{1/2}$(**Bdp6**) is also consistent with the idea that dialkylaniline is a slightly better donor than triarylamine. The fact that $E_{1/2}$(**Bdp8**) ~ $E_{1/2}$(**Bdp5**) also suggests that the relative position of the donor substituents introduced on the aza-BODIPY core (above or below) has no significant influence on its electron density. This conclusion was also confirmed by the electrochemical data collected for the tetra-substituted derivatives with $E_{1/2}$(**Bdp9**) ~ $E_{1/2}$(**Bdp10**).

The data collected in Table 2 also reveals that the BODIPY core is significantly easier (~40 mV) to reduce in **Bdp9** and **Bdp10** than in **Bdp5** and **Bdp8**, suggesting that two EDGs have a stronger electron effect on the aza-BODIPY core than four. This unexpected result can potentially be explained by steric repulsions between the 3,5-phenyl and 2,6-thiophene rings resulting in a twist of those groups with respect to the aza-BODIPY plane, which is a trend found by DFT optimizations.

Bdp5 and **Bdp9** were then subjected to spectroelectrochemistry (SEC) measurements (Figure 5) conducted in a thin-layer cell (0.5 mm) using a platinum grid as working electrode.

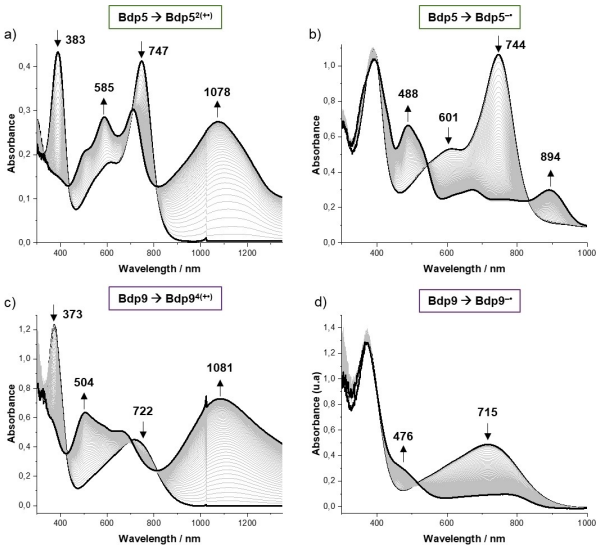

Figure 5. UV-vis-NIR spectra recorded over time in a thin-layer spectroelectrochemical cell (0.5 mm, Pt grid) for solutions of **Bdp5** or **Bdp9** when the potential of the platinum grid was swept linearly from E_{ocp} a) to the first oxidation of **Bdp5** at 0.65 V; b) to the first reduction of **Bdp5** at −0.85 V; c) to the first oxidation of **Bdp9** at 0.65 V; d) to the first reduction of **Bdp9** at −0.90 V. E vs. $AgNO_3$/Ag (10^{-2} M in ACN), all measurements carried out in dichloroethane + 0.1 M TBAP.

The absorption spectra recorded over time with **Bdp5** upon scanning (20 mV/s) the potential of the working electrode from 0 to 0.65 V are shown in Figure 5. Oxidation of the terminal amines was found to result in the gradual decrease in the intensity of the band at λ_{max} = 380 nm in favor of a very intense and broad band developing in the NIR region from 800 nm to 1300 nm (Figure 5a). The main absorption band centered at 747 nm was also found to undergo a significant loss of intensity accompanied by an hypsochromic shift of the λ_{max} value down to 709 nm. Oxidation of the terminal amines yielding **Bdp5**$^{2(+\bullet)}$ also led to a significant increase in the intensity of the ICT band observed between 450–650 nm, suggesting a good electronic communication between the amine and the aza-BODIPY core. As expected, very similar behaviors were observed with the structural analogue **Bdp9**, exhibiting four thiophene-triarylamine moieties connected to the same aza-BODIPY platform (Figure 5c), including the same broad band centered at λ_{max} = 504 nm but with a much greater relative intensity consistent with the increase in the number of amine functions.

Similar spectroscopic measurements were then carried out focusing on the BODIPY-centered one electron reduction of **Bdp5** and **Bdp9**. As can be seen in Figure 5b, the in situ formation of **Bdp5**$^{-\bullet}$ led to a decrease of the initial bands centered at λ_{max} = 601 (ICT) and 744 (Cy) nm and to the concomitant development of two new signals at λ_{max} = 488 nm and 894 nm. These data, showing a complete disappearance of the characteristic ICT and Cy bands at the end of the experiment, are thus in full agreement with the proposed attribution of the electron transfer on the aza-BODIPY unit. Then, the observation of clean isosbestic points at 544 et 834 nm

demonstrates the stability of **Bdp5**$^{-\bullet}$ at the time scale of the measurement.

Similar measurements carried out on the tetraamino-substituted analogue **Bdp9** led to similar evolutions including a disappearance of the Cy band at 715 nm in favor of a set of weakly intense signals observed between 450 and 900 nm attributed to the formation of **Bdp9**$^{-\bullet}$.

Computational calculations

We have performed theoretical calculations using a protocol accounting for solvation effects and combining second-order coupled-cluster (CC2) and time-dependent density functional theory (TD-DFT), that is detailed in the Supporting Information For the emissive dyes, one can obtain physically-sound comparison between theory and experiment when using 0—0 energies.[44] The theoretical best estimates are 1.73, 1.75, 1.71, 1.68, and 1.78 eV for **Bdp1**^{b}, **Bdp5**, **Bdp6**, **Bdp7**, and **Bdp8**, respectively (Table S4) leading to a mean absolute error of 0.11 eV with respect to the measurements, which is acceptable. Globally the measured trends are also nicely reproduced with **Bdp7** (**Bdp8**) the most redshifted (blueshifted) of the series in both theory and experiment. Interestingly, as can be seen in Table S4, besides the lowest intense S_0-S_1 absorption band that mainly presents a BODIPY-centered nature (see below), theory also foresees significant absorption ca. 100 nm blueshifted compared to this main transition due to the close-lying S_0–S_2 and S_0–S_3 transitions both involving strong ICT (see below). This indicates that the shoulder/peak appearing experimentally in the 550–650 nm region of the absorption spectra (Figure 2) are likely a combination of vibronic effects from the S_0–S_1 band and the excitations towards two higher-lying electronic states.

Selected transitions are represented in Figure 6 under the form of electron density difference plots (see the Supporting Information for full data). One clearly notices that the S_0–S_1 transition has the typical aza-BODIPY topology which is reminiscent of cyanine transitions. There is nevertheless a small ICT component, that is significantly larger in **Bdp7** than **Bdp5**, with increase of dipole moment during the transition of +0.37 D and +3.63 D, respectively, which perfectly fits the experimental trends. The higher-lying transitions show a significant ICT character (in **Bdp5**) and even a much stronger one (in **Bdp7**), consistent with the shapes of the experimental spectra in that spectral region (much less resolved for the latter dye). Interestingly, Figure 5 also shows that the thiophene acts as secondary donor, slightly for the third state of **Bdp5** but strongly for both the S_0–S_2 and S_0–S_3 transitions of **Bdp7**. Having a strong primary donor group therefore enhances the impact of the thiophene in the present series. As can be seen in Figure S11, the situation is rather similar for **Bdp8**, with ICT in the second and third transitions, logically coming from the "top" moieties of the compound. Interestingly in **Bdp9**, theory foresees that the ICT are more induced by both the top Ph-OAlk groups and the EDG locates at positions 2 and 6, whereas the bottom triphenylamine units seem of relatively low importance. In contrast in **Bdp10**, that is both top and side substituted, the

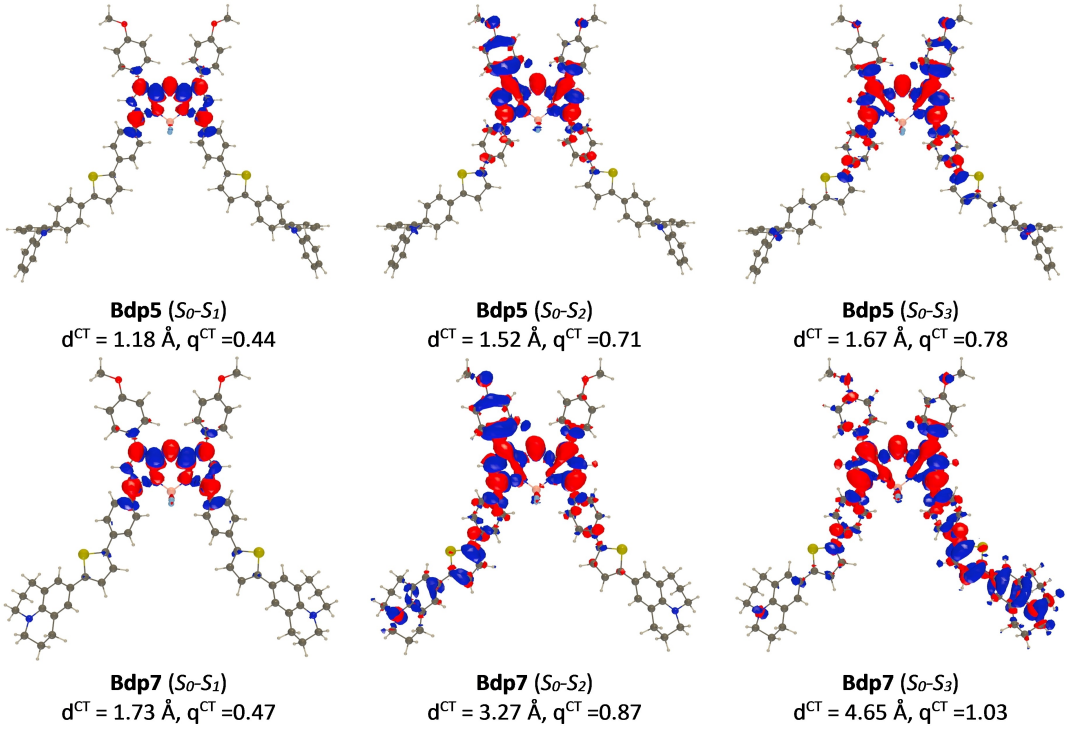

Figure 6. Electron density difference plots for the lowest absorptions of all compounds. Blue and red lobes correspond to regions of decrease and increase of density upon absorption, respectively. The CT parameters are indicated as well. Representations for all states can be found in the Supporting Information.

substituents at the top seems to be mainly responsible for the ICT character of both the S_0-S_2 and S_0-S_3 transitions.

For **Bdp7**, we used theory (see the Supporting Information for details) to estimate the relative energies of the relaxed structures of the three lowest excited states in both toluene and DCM. In the former, the relaxed cyanine state (S_1) is estimated to be 0.27 eV more stable than the relaxed ICT states (S_2 and S_3 that are nearly degenerated in our calculations). In contrast in DCM, the relaxed ICT (S_2 and S_3) states are only 0.05 eV less stable than the relaxed S_1. Whilst this does not perfectly fit experiments that finds an accessible ICT state in DCM (see above), such small 0.05 eV difference is clearly smaller than the theoretical incertitude. At least, our calculations confirm that the two states become close even in an averagely polar medium.

We have also modelled **Bdp5**$^{-\bullet}$ and **Bdp5**$^{2(+\bullet)}$ in an effort to help interpreting the spectro-electrochemistry experiments (Figure 7). As can be seen on the spin density plots shown in the Supporting Information, the additional electron is confined within the BODIPY core in **Bdp5**$^{-\bullet}$, whereas the electrons are mainly extracted from the two triphenylamine groups in **Bdp5**$^{2(+\bullet)}$ yet with a spin density that is much more delocalized in this dication. For **Bdp5**$^{-\bullet}$, as can be seen in Table S5, TD-DFT yields: *i)* a moderately intense band ($f=0.46$) at 763 nm, that is redshifted by 116 nm as compared to the intense band of **Bdp5** (647 nm, $f=1.27$), consistent with the band emerging at ca. 900 nm experimentally (Figure 5b, this additional peak is redshifted by ca. 150 nm as compared to the neutral closed-shell structure); *ii*) no significant absorption in the 500–700 nm region; *iii*) several bright transitions in the 350–450 domain (also in line with the measurements). For **Bdp5**$^{2(+\bullet)}$, three excited states are predicted above 900 nm (Table S5), with a particularly intense one at 1077 nm ($f=1.53$) consistent with the experiment, see Figure 5a. The intense band of **Bdp5** (647 nm, $f=1.27$) disappears but **Bdp5**$^{2(+\bullet)}$ presents a less intense absorption in that region (665 nm, $f=0.31$), as well as a series of bright transitions in the 500–600 nm domain, absent in **Bdp5** (Table S5), again consistent with the experimental findings. For the radical anion, the additional band corresponds to an excited state presenting globally the same topology as in the neutral compound, consistent with the rather moderate redshift. In contrast, in **Bdp5**$^{2(+\bullet)}$ the transition mainly responsible for the additional strongly redshifted band involves a large ICT from towards the electron-deficient triphenylamine units, this strong ICT nature being consistent with the broadness of the experimental band.

Conclusions

In summary, we successfully synthesized a series of new push-pull aza-BODIPY derivatives, **Bdp5-10**, containing thiophene unit acting as π-conjugated spacer and investigated the impact of the position and of the EDGs on the NLO properties. **Bdp6** and **Bdp7** exhibit redshifted absorption spectra and present a much more intense ICT band compared to previously reported analogues. Such large increase of the intramolecular charge transfer process results from the presence of thiophene moieties that increase the electronic π-conjugation and act as strong auxiliary donors. Electrochemical measurements confirmed these observations and also revealed the remarkable stability of the electro-generated species. The strong fluorescence quenching observed for **Bdp5** to **Bdp6** with increasing solvent polarity indicates an ultrafast excited state relaxation towards the ICT state. In addition, the synthetic pathway used to introduce the nitrogen-based donor groups, involving palladium-catalyzed Stille cross-coupling reaction, made the tetra-functionalization possible. Both dyes **Bdp9** and **Bdp10** are currently the only aza-BODIPY that are substituted with EDG in both 3,5 or 1,7 and 2,6 peripherical positions. This achievement leads to promising results with broad absorption band as a consequence of an improved ICT. Then, this new series of thiophene derivatives fulfills the prerequisites in order to consider them for future NLO investigations. Furthermore, these dyes display suitable properties to be potentially implemented in optoelectronic devices, such as dye sensitized (DSSC) or organic solar cells (OSC).

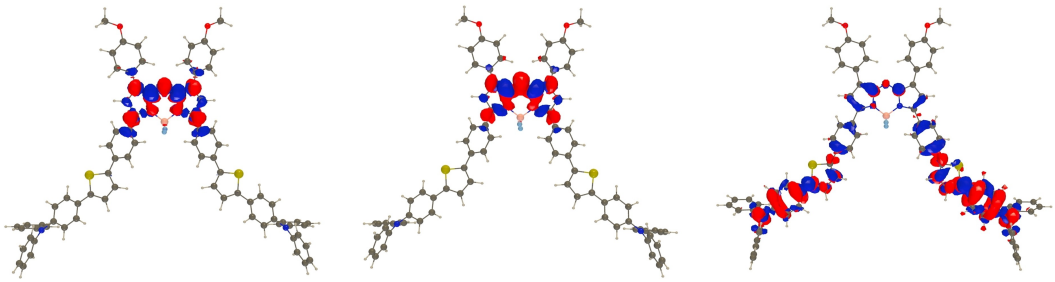

Figure 7. Electron density difference plots for the lowest significantly-allowed excitations of **Bdp5** under various forms. See caption of Figure 5 for more details.

Acknowledgements

The authors acknowledge the Direction Générale de l'Armement (DGA) and Thales LAS for financial support and for the grants of T.B. and V.M. in Pro-IR project. D.J. is indebted to the CCIPL/GliciD computational center installed in Nantes for the generous allocation of computational resources.

Conflict of Interests

The authors declare no potential conflict of interest.

Data Availability Statement

The data that support the findings of this study are available from the corresponding author upon reasonable request.

Keywords: aza-BODIPY · electrochemistry · fluorescence · intramolecular charge transfer (ICT) · thiophene

[1] C. Yin, X. Li, Y. Wang, Y. Liang, S. Zhou, P. Zhao, C.-S. Lee, Q. Fan, W. Huang, *Adv. Funct. Mater.* **2021**, *31*, 2104650.
[2] Y. Su, B. Yu, S. Wang, H. Cong, Y. Shen, *Biomaterials* **2021**, *271*, 120717.
[3] P. Chinna Ayya Swamy, G. Sivaraman, R. N. Priyanka, S. O. Raja, K. Ponnuvel, J. Shanmugpriya, A. Gulyani, *Coord. Chem. Rev.* **2020**, *411*, 213233.
[4] G. P. Kini, S. J. Jeon, D. K. Moon, *Adv. Funct. Mater.* **2021**, *31*, 2007931.
[5] F. Grifoni, M. Bonomo, W. Naim, N. Barbero, T. Alnasser, I. Dzeba, M. Giordano, A. Tsaturyan, M. Urbani, T. Torres, C. Barolo, F. Sauvage, *Adv. Energy Mater.* **2021**, *n/a*, 2101598.
[6] W. Naim, V. Novelli, I. Nikolinakos, N. Barbero, I. Dzeba, F. Grifoni, Y. Ren, T. Alnasser, A. Velardo, R. Borrelli, S. Haacke, S. M. Zakeeruddin, M. Graetzel, C. Barolo, F. Sauvage, *JACS Au* **2021**, *1*, 409–426.
[7] T. Baron, W. Naim, I. Nikolinakos, B. Andrin, Y. Pellegrin, D. Jacquemin, S. Haacke, F. Sauvage, F. Odobel, *Angew. Chem. Int. Ed.* **2022**, *61*, e202207459.
[8] T. Baron, X. Zarate, Y. Hidalgo-Rosa, M. Zambrano-Angulo, K. Mall-Haidaraly, R. Pino-Rios, Y. Pellegrin, F. Odobel, G. Cárdenas-Jirón, *Comptes Rendus. Chimie* **2021**, *24*, 1–14.
[9] C. Shi, J. B. Wu, D. Pan, *J. Biomed. Opt.* **2016**, *21*, 50901.
[10] L. Beverina, P. Salice, *Eur. J. Org. Chem.* **2010**, *2010*, 1207–1225.
[11] E. B. Knott, *J. Chem. Soc. (Resumed)* **1947**, *0*, 1196–1201.
[12] J. Wang, N. Boens, L. Jiao, E. Hao, *Org. Biomol. Chem.* **2020**, *18*, 4135–4156.
[13] F. Ceugniet, Q. Huaulmé, A. Sutter, D. Jacquemin, N. Leclerc, G. Ulrich, *Chem. Eur. J.* **2022**, *28*, e202200130.
[14] H. Lu, J. Mack, Y. Yang, Z. Shen, *Chem. Soc. Rev.* **2014**, *43*, 4778–4823.
[15] L. Wang, Z. Xiong, X. Ran, H. Tang, D. Cao, *Dyes Pigm.* **2022**, *198*, 110040.
[16] T. Weil, T. Vosch, J. Hofkens, K. Peneva, K. Müllen, *Angew. Chem. Int. Ed.* **2010**, *49*, 9068–9093.
[17] S. Pascal, S. David, C. Andraud, O. Maury, *Chem. Soc. Rev.* **2021**, *50*, 6613–6658.
[18] G. S. He, L.-S. Tan, Q. Zheng, P. N. Prasad, *Chem. Rev.* **2008**, *108*, 1245–1330.
[19] M. Pawlicki, H. A. Collins, R. G. Denning, H. L. Anderson, *Angew. Chem. Int. Ed.* **2009**, *48*, 3244–3266.
[20] P.-A. Bouit, K. Kamada, P. Feneyrou, G. Berginc, L. Toupet, O. Maury, C. Andraud, *Adv. Mater.* **2009**, *21*, 1151–1154.
[21] R. S. Rao, B. Yadagiri, G. D. Sharma, S. P. Singh, *Chem. Commun.* **2019**, *55*, 12535–12538.
[22] S. Pascal, Q. Bellier, S. David, P.-A. Bouit, S.-H. Chi, N. S. Makarov, B. Le Guennic, S. Chibani, G. Berginc, P. Feneyrou, D. Jacquemin, J. W. Perry, O. Maury, C. Andraud, *J. Phys. Chem. C* **2019**, *123*, 23661–23673.
[23] D. Château, Q. Bellier, F. Chaput, P. Feneyrou, G. Berginc, O. Maury, C. Andraud, S. Parola, *J. Mater. Chem. C* **2014**, *2*, 5105–5110.
[24] S. David, D. Chateau, H.-J. Chang, L. H. Karlsson, M. V. Bondar, C. Lopes, B. Le Guennic, D. Jacquemin, G. Berginc, O. Maury, S. Parola, C. Andraud, *J. Phys. Chem. C* **2020**, *124*, 24344–24350.
[25] S. David, H.-J. Chang, C. Lopes, C. Brännlund, B. Le Guennic, G. Berginc, E. Van Stryland, M. V. Bondar, D. Hagan, D. Jacquemin, C. Andraud, O. Maury, *Chem. Eur. J.* **2021**, *27*, 3517–3525.
[26] H.-J. Chang, M. V. Bondar, N. Munera, S. David, O. Maury, G. Berginc, B. Le Guennic, D. Jacquemin, C. Andraud, D. J. Hagan, E. W. Van Stryland, *Chem. Eur. J.* **2022**, *28*, e202104072.
[27] X. Zhang, H. Yu, Y. Xiao, *J. Org. Chem.* **2012**, *77*, 669–673.
[28] Q. Bellier, F. Dalier, E. Jeanneau, O. Maury, C. Andraud, *New J. Chem.* **2012**, *36*, 768–773.
[29] S. Zheng, A. Leclercq, J. Fu, L. Beverina, L. A. Padilha, E. Zojer, K. Schmidt, S. Barlow, J. Luo, S.-H. Jiang, A. K.-Y. Jen, Y. Yi, Z. Shuai, E. W. Van Stryland, D. J. Hagan, J.-L. Brédas, S. R. Marder, *Chem. Mater.* **2007**, *19*, 432–442.
[30] A. Gorman, J. Killoran, C. O'Shea, T. Kenna, W. M. Gallagher, D. F. O'Shea, *J. Am. Chem. Soc.* **2004**, *126*, 10619–10631.
[31] S. David, G. Pilet, G. Berginc, C. Andraud, O. Maury, *New J. Chem.* **2020**, *44*, 13125–13130.
[32] R. Gresser, H. Hartmann, M. Wrackmeyer, K. Leo, M. Riede, *Tetrahedron* **2011**, *67*, 7148–7155.
[33] M. Fontani, E. Garoni, A. Colombo, C. Dragonetti, S. Fantacci, H. Doucet, J.-F. Soulé, J. Boixel, V. Guerchais, D. Roberto, *Dalton Trans.* **2018**, *48*, 202–208.
[34] S. Gao, T. K. Bethel, T. Kakeshpour, G. E. Hubbell, J. E. Jackson, J. J. Tepe, *J. Org. Chem.* **2018**, *83*, 9250–9255.
[35] Q. Bellier, S. Pégaz, C. Aronica, B. L. Guennic, C. Andraud, O. Maury, *Org. Lett.* **2011**, *13*, 22–25.
[36] E. Ishow, G. Clavier, F. Miomandre, M. Rebarz, G. Buntinx, O. Poizat, *Phys. Chem. Chem. Phys.* **2013**, *15*, 13922–13939.
[37] V. Maffeis, R. Brisse, V. Labet, B. Jousselme, T. Gustavsson, *J. Phys. Chem. A* **2018**, *122*, 5533–5544.
[38] T. Inari, M. Yamano, A. Hirano, K. Sugawa, J. Otsuki, *J. Phys. Chem. A* **2014**, *118*, 5178–5188.
[39] E. Fron, M. Lor, R. Pilot, G. Schweitzer, H. Dincalp, S. D. Feyter, J. Cremer, P. Bäuerle, K. Müllen, M. V. der Auweraer, F. C. D. Schryver, *Photochem. Photobiol. Sci.* **2005**, *4*, 61–68.
[40] A. B. Nepomnyashchii, A. J. Bard, *Acc. Chem. Res.* **2012**, *45*, 1844–1853.
[41] S. Pascal, L. Bucher, N. Desbois, C. Bucher, C. Andraud, C. P. Gros, *Chem. Eur. J.* **2016**, *22*, 4971–4979.
[42] T. Li, T. Meyer, R. Meerheim, M. Höppner, C. Körner, K. Vandewal, O. Zeika, K. Leo, *J. Mater. Chem. A* **2017**, *5*, 10696–10703.
[43] B. Tang, J. Zhao, J.-F. Xu, X. Zhang, *Chem. Sci.* **2020**, *11*, 1192–1204.
[44] P.-F. Loos, D. Jacquemin, *ChemPhotoChem* **2019**, *3*, 684–696.

Manuscript received: April 28, 2023
Accepted manuscript online: June 5, 2023
Version of record online: July 24, 2023